Magneto-Optical Observation of Picosecond Dynamics of Single Nanomagnets

ARTICLE *in* NANO LETTERS · JANUARY 2007

Impact Factor: 13.59 · DOI: 10.1021/nl0623457 · Source: PubMed

NANO LETTERS

2006
Vol. 6, No. 12
2939−2944

Magneto-Optical Observation of Picosecond Dynamics of Single Nanomagnets

Anjan Barman,[†] Suqin Wang,[†] Jeffrey D. Maas,[‡] Aaron R. Hawkins,[‡] Sunghoon Kwon,[§,||] Alexander Liddle,[§] Jeffrey Bokor,[§] and Holger Schmidt*,[†]

School of Engineering, University of California Santa Cruz, 1156 High Street, Santa Cruz, California 95064, ECEn Department, Brigham Young University, 459 Clyde Building, Provo, Utah 84602, and Molecular Foundry, Lawrence Berkeley National Laboratory, Berkeley, California 94720

Received October 5, 2006; Revised Manuscript Received November 2, 2006

ABSTRACT

We report measurements of picosecond dynamics of individual nickel nanomagnets as a function of magnet dimension, aspect ratio, and magnetic environment. Spatial sensitivity to nanomagnet diameters as small as 125 nm is achieved by use of cavity enhancement of the magneto-optic Kerr effect (CE-MOKE). The importance of single-particle measurements without ensemble effects for extracting the size dependence of the intrinsic nanomagnet material properties is demonstrated.

In recent years, nanomagnet research has evolved into a diverse field with increasingly multidisciplinary applications. Initially, much work focused on obvious areas such as patterned magnetic media for data storage,[1] magnetic memory (MRAM),[2] and logic.[3] More recently, exciting biomedical applications of nanomagnets including MRI enhancement[4] and "magnetic virus" sensors[5] have emerged. More applications are certain to follow, for example, genetically engineered nanomagnet arrays[6] or localized magnetic fields on a chip. A thorough understanding of the material properties is essential for utilization of nanomagnets in any application. This is particularly exciting as new effects such as transitions to the single magnetic domain and superparamagnetic[7] regimes come into play as magnet size approaches the deep nanometer scale. Consequently, new experimental techniques need to be developed that reveal the material properties of individual magnetic nanoparticles without ensemble effects that may mask intrinsic behavior in nanomagnet arrays. These include particle inhomogeneities, signal reduction due to opposing magnetization directions in unsaturated arrays, averaging over phase and kinetic pathways in dynamic processes, magnetostatic interactions, and others. An understanding of dynamic properties is necessary for virtually all applications.

Several techniques have been applied to studying single magnetic particles. At one extreme are inherently slow methods with high spatial resolution such as magnetic force microscopy,[8] spin-polarized scanning tunneling microscopy,[9] Lorentz force microscopy,[10] and spin-polarized low-energy electron microscopy.[11] At the other extreme, sub-nanosecond temporal resolution on the microscale has been demonstrated with Brillouin light scattering,[12,13] ferromagnetic resonance,[14,15] time-resolved Kerr microscopy,[16−21] and inductive techniques.[22] The best spatiotemporal sensitivities were obtained with magnetoresistive methods,[23,24] X-ray microscopy,[25] and time-resolved magneto-optic Kerr effect (MOKE).[21] Recently, precessional dynamics from nanomagnet ensembles has been explored using Brillouin light scattering[26] and time-resolved Kerr microscopy[27,28] with superior temporal resolution (∼100 fs). However, recording such processes from individual magnets with simultaneous sub-picosecond resolution and nanometer sensitivity remains challenging, and no studies of magnetization dynamics in individual nanomagnets in the single-domain regime with sub-picosecond resolution have been reported yet.

Here, we report the first measurements of ultrafast magnetization dynamics of individual nickel nanomagnets. Recent work on quasi-static magnetization switching has built on the well-known increase in the MOKE signal from magnetic surfaces coated by a suitable dielectric layer.[29] A substantial increase in areal sensitivity down to individual single-domain nanomagnets using cavity-enhanced MOKE (CE-MOKE) was observed.[30] We demonstrate that the additional fabrication steps required for cavity enhancement do not affect the dynamic material properties, making CE-

* Corresponding author. E-mail: hschmidt@soe.ucsc.edu.
[†] School of Engineering, University of California Santa Cruz.
[‡] ECEn Department, Brigham Young University.
[§] Molecular Foundry, Lawrence Berkeley National Laboratory.
[||] Present address: School of Electrical Engineering, Seoul National University.

10.1021/nl0623457 CCC: $33.50
Published on Web 11/15/2006

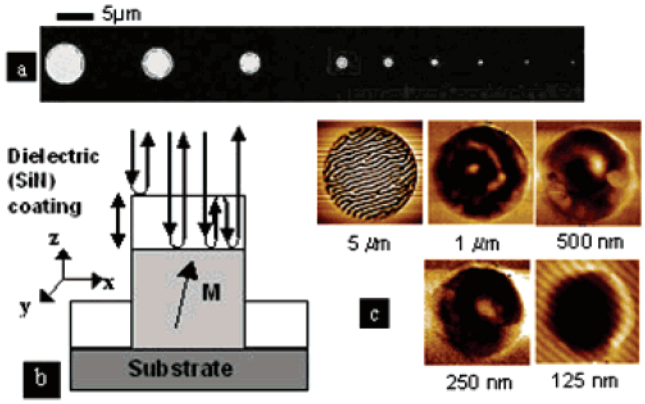

Figure 1. Nanomagnet sample and experimental setup: (a) scanning electron microscope images of the samples; (b) schematic of the cavity enhancement of MOKE; (c) magnetic force microscope images of single magnets of various diameters.

MOKE a viable and attractive technique for studying dynamic magnetic properties of materials on the nanoscale. We use this technique to study magnetization precession in individual nickel nanomagnets as a function of diameter and aspect ratio (AR), covering the transition from the microscale to the single-domain regime. We demonstrate that the transition to the single-domain regime in small magnets is accompanied by a significant speedup of the dynamic response. Finally, we show that the details of this behavior can only be observed in single magnets, but not in a dense array.

The magnetic elements (circular nickel cylinders on silicon substrate) were fabricated by electron-beam lithography and electron-beam deposition[30] with thicknesses of 150 nm and diameters between 5 μm and 125 nm. Consequently, their physical shape varies between disklike and postlike and aspect ratio (AR) from 0.03 to 1.2. It is well-known that static magnetic properties depend strongly on aspect ratio, and the range investigated here allows us to study the effects on the dynamics. The magnets were optically and magnetostatically isolated as shown in the scanning electron micrographs (Figure 1a). One batch of magnets was coated with a 70 nm thick silicon nitride (SiN) layer using low-temperature plasma-enhanced chemical vapor deposition (Figure 1b). Multiple reflections in the SiN layer result in a 5-fold increase of polarization rotation of light reflected from the nanomagnet. Simultaneously, the reflection coefficient of the substrate is reduced by an order of magnitude compared to the uncoated samples. The combination of the two effects improves the spatial sensitivity by both enhancing the Kerr rotation and reducing the background noise.[30] Magnetic force microscope (MFM) images from selected magnetic elements at zero bias field are shown in Figure 1c. Magnets larger than 500 nm show multiple domains. The 250 nm magnet is nearly single domain while the 125 nm magnet appears fully single domain.

The experimental setup for dynamic measurements is based on a two-color optical pump−probe technique (see Supporting Information for a schematic). The magnets were optically pumped by linearly polarized laser pulses (15 mW at 400 nm, pulsewidth 100 fs, repetition rate 76 MHz). The

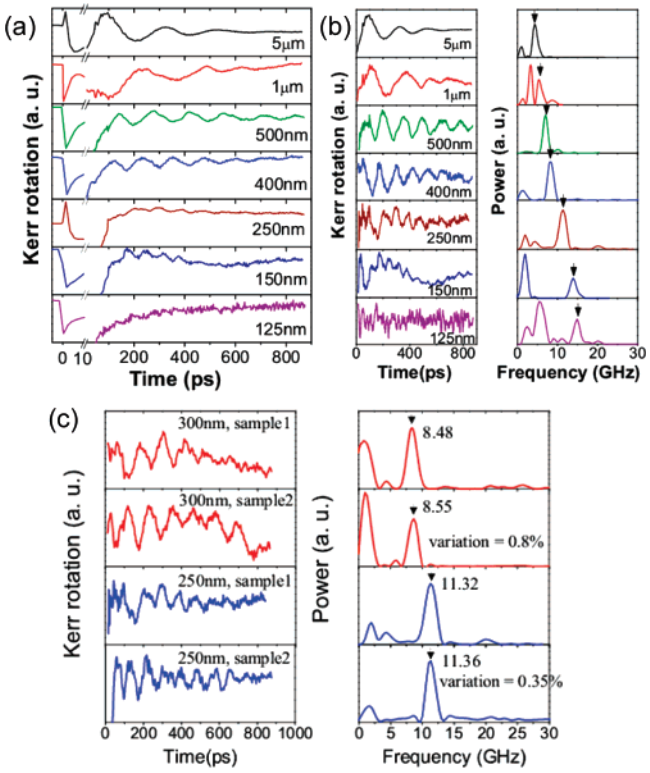

Figure 2. Measurements of the time-resolved Kerr rotation and the corresponding fast Fourier transform (FFT) spectra: (a) time-resolved Kerr rotations (raw data) for single magnets of varying diameter at $H_{bias} = 1.68$ kOe. The horizontal scale is broken between 10 and 15 ps for showing three different regions clearly; (b) time-resolved Kerr rotations after subtracting a double exponential background (left panels) and FFT spectra (right panels) at $H_{bias} = 1.68$ kOe with arrows indicating the uniform precession frequencies; (c) left, representative time traces for four different nanomagnets in the range of frequency jump (aspect ratio 0.6); right, corresponding frequency response indicating magnitude of intraparticle (same size) and interparticle (different size) variation.

sudden heating by the pump pulse perturbs the magnetization instantaneously and causes an internal anisotropy field pulse.[21] This results in a change in the equilibrium magnetization orientation and triggers a precession. 2 mW linearly polarized laser pulses of 800 nm wavelength were time delayed with respect to the pump beam to probe the magnetization dynamics by detecting the polar magneto-optical Kerr rotation. The temporal evolution of magnetization was built point by point by varying the optical delay between the pump and probe. The pump beam was chopped at 2 kHz and lock-in detection was used. Pump and probe beams were focused down to 0.98 μm diameter spots and precisely overlapped at the center of the sample at normal incidence using a single microscope objective (N.A. = 0.66). Spectral filtering before probe detection eliminated the back-reflected pump beam.

First, we focus on demonstrating the utility of CE-MOKE to observe the dynamics of single nanomagnets. The time-resolved dynamics are shown (Figure 2a) from individual SiN-coated magnets with diameter between 5 μm and 125 nm in a perpendicular static magnetic bias field $H_{bias} = 1.68$ kOe. The time scale is broken between 10 and 15 ps to show three different regimes. The first 10 ps shows fast demag-

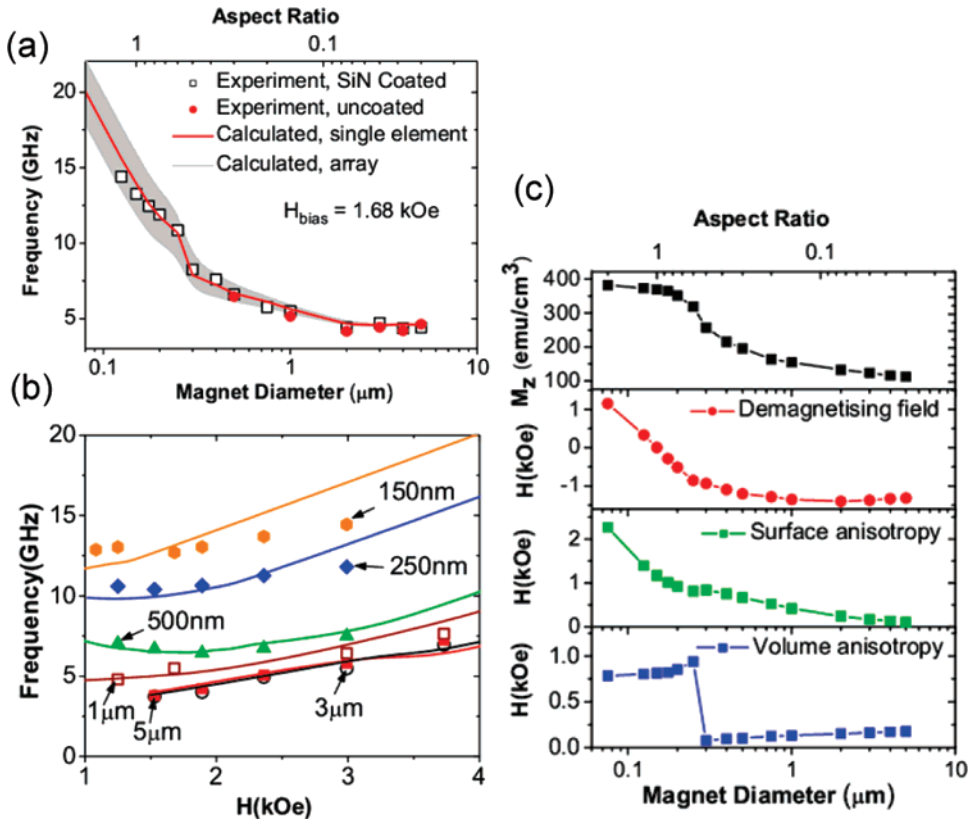

Figure 3. Theoretical modeling of the diameter and bias-field dependence of experimentally obtained precession frequencies. (a) Experimentally obtained frequencies of the uniform precession modes from uncoated and 70 nm SiN-coated magnets as a function of magnet diameter (aspect ratio) at H_{bias} = 1.68 kOe. Solid line: calculated precession frequencies of single magnets from eq 1. The gray shaded region shows the possible range of precession frequencies in arrays of magnets separated by 56 nm. (b) Experimental (points) and calculated (curves) precession frequencies as a function of bias magnetic field (H_{bias}). (c) M_z and contributions of different terms in eq 1 as a function of magnet diameter (aspect ratio).

netization and a quick recovery with time constants between 1 and 10 ps. This shows that the bandwidth of our all-optical technique is determined by the inverse laser pulsewidth (100 fs) similar to ref 21. The oscillatory signal indicating the precession is observed on top of an exponential decay.

The signals are shown after subtracting a double exponential background (Figure 2b, left panels), and the right panels (Figure 2b) show their fast Fourier transform (FFT) spectra. Multiple frequencies are observed for almost all samples. The dynamics can have different low-frequency contributions in addition to the uniform mode (coherent precession of spins), such as magnetostatic modes due to spatial inhomogeneities (5−1 μm), vortex-state dynamics (750−150 nm), and low-frequency measurement noise (125 nm). Modes at higher frequencies could correspond to higher order perpendicular spin waves or forward volume magnetostatic (FWVMS) modes, but are not observed. Due to the confinement of the pump pulse to the vicinity of the sample surface (~10 nm), higher order modes are excited with much smaller amplitude and typically only the first mode is excited.[21] In our sample, the frequency of this mode would differ from the uniform mode by less than 0.5 GHz so that it will not be resolved given its small amplitude and the width of the fundamental mode. The absence of clear FWVMS modes is also likely due to their small amplitudes. Here, we focus on the uniform mode dynamics after 10 ps indicated by the arrows (Figure 2b). These frequencies are directly compared as a function of magnet diameter (AR) for both uncoated and SiN-coated Ni magnets with identical dimensions (Figure 3a). Two conclusions can be drawn. First, the precession frequencies remain unaffected by the SiN coating, demonstrating the noninvasive nature of the cavity enhancement of MOKE. Second, for uncoated magnets no precessional signal was detectable below 500 nm due the signal-to-noise reduction with cross-sectional area.[30] This shows the applicability of the cavity enhancement technique for resolving magnetization dynamics of individual nanomagnets down to the single domain regime.

Next, we analyze the dynamic behavior of the nanomagnets as a function of magnet dimensions, shape, and AR as they undergo the transition to the single-domain regime. The frequency response versus magnet diameter (AR) shows three different regimes (Figure 3a). Between 5 μm (AR = 0.03) and 2 μm (AR = 0.075) the frequency remains almost constant. Below 1 μm (AR = 0.15) the frequency increases steadily with reducing diameter down to 300 nm (AR = 0.5). At 250 nm (AR = 0.6) the frequency undergoes a sharp jump by 33% and then increases at a steeper rate down to 125 nm (AR = 1.2). This step is clearly a physical phenomenon as the frequency variation between different magnets of the same size is less than 1% as shown in Figure 2c, where the frequency response for four individual nanomagnets (two at

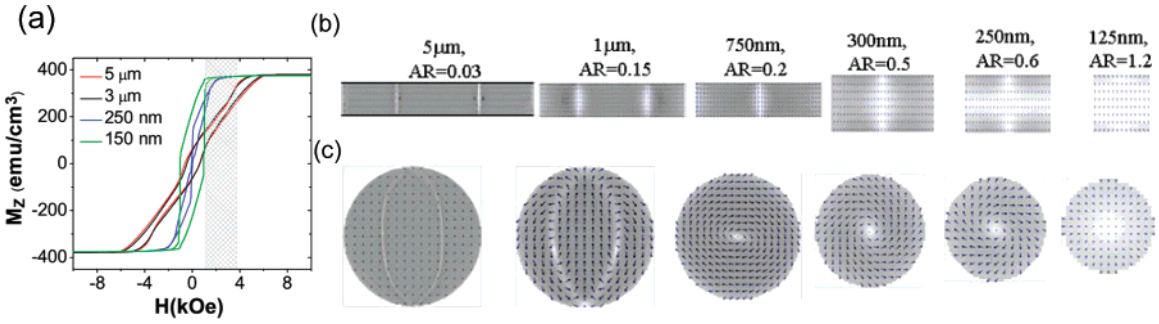

Figure 4. Simulated hysteresis loops and static micromagnetic images of the studied nanomagnets. (a) Simulated hysteresis loops for magnets of four different diameters with the gray shaded area showing the experimentally accessed range of H_{bias}. Simulated images are shown as a function of magnet diameter (aspect ratio). The grayscale and arrows represent the out-of-plane component of magnetization (M_z). The arrows are subsampled over a number of cells for visual clarity. The physical size of the samples is scaled arbitrarily to fit them into the figure. (b) Side view and (c) top view of the magnets. The 125 nm sample shows fully single domain behavior where all spins are essentially parallel; i.e., their main components are aligned in the same direction.

300 nm and two at 250 nm) is compared. In order to fully characterize this behavior, we also measured the time-resolved dynamics as a function of external bias field H_{bias}. The precession frequency is plotted as a function of H_{bias} up to 3.73 kOe (Figure 3b). Magnets with diameter $\geq 2\ \mu$m (AR ≤ 0.075) exhibit a monotonic increase in the precession frequency whereas magnets with 250 and 500 nm diameter show a dip at intermediate field values. The latter suggests a competition between different magnetic fields acting on the sample that requires a combination of dynamic and static analyses. The magnetization precesses around an effective magnetic field given by $H_{eff} = -(1/M)(\nabla_u E_{eff})$, where E_{eff} is the effective magnetic energy consisting of several contributions. We model the precession frequency by solving the Landau−Lifshitz equation[31] in the small angle approximation and expressing the effective magnetic field as $H_{eff} = H_{bias} + H_{demag} + H_{ani} + H_{off}$. H_{demag} is the demagnetizing field due to shape anisotropy, H_{ani} is the total anisotropy field (including volume and surface contributions), and H_{off} includes additional fields such as an optically induced effective pulsed field, stray fields from the experimental components, and possible errors in determining H_{bias}. The demagnetizing energy per unit volume is given by $(N_x M^2 u_x^2 + N_y M^2 u_y^2 + N_z M^2 u_z^2)/2$, where N_x, N_y, and N_z are the three components of the demagnetizing tensor which depend on aspect ratio (for our circular cylinders $N_x = N_y = 0.5(4\pi - N_z)$), M is the magnetization, and u is the unit vector.[32] We have considered two different contributions to the anisotropy energy, the volume anisotropy energy, $-K_{uz}\cdot u_z^2$, and the surface anisotropy energy, $[-(2K_{S1}\cdot u_z^2)/t - (2K_{S2}\cdot u_z^2)/d]$, where K_{uz} is the volume anisotropy constant, K_{S1} and K_{S2} are anisotropy constants for the roughness and defects for the top/bottom and side surface of the magnet, and t and d refer to magnet thickness and diameter, respectively. The constant thickness, $t = 150$ nm, of all samples ensured that the first term "$-(2K_{S1}\cdot u_z^2)/t$" is independent of AR and may be included in the volume anisotropy energy. Hence, we write an effective volume anisotropy energy $-K_1\cdot u_z^2$, where $K_1 = (K_{uz} + 2K_{S1}/t)$. Assuming the above expression for the effective field the precession frequency is given by

$$f = \frac{g\mu_B}{h}\left[H_{bias} + (N_x - N_z)M_z + \frac{4K_{s2}}{dM_z} + \frac{2K_1}{M_z} + H_{off}\right] \quad (1)$$

where g is the Lande "g" factor, μ_B is the Bohr magneton, and h is Planck's constant. Clearly, the out-of-plane magnetization component M_z has a significant influence on the precession frequency. M_z values were therefore obtained from micromagnetic simulations of the static magnetic configurations using object oriented micromagnetic framework (OOMMF) software.[33] The magnets were discretized into parallelepipeds with sides smaller than the exchange length (21 nm) of nickel, and hysteresis loops for M_z were calculated (Figure 4a), using a saturation magnetization of 484 emu/cm^3, an exchange constant of 9×10^{-7} erg/cm, and $g = 2.21$. The side view (Figure 4b) and top surface (Figure 4c) of the resulting magnetostatic configurations of the magnets for $H_{bias} = 1.68$ kOe are shown.

The grayscale and the arrows represent a spatial map of M_z. Magnets between 5 and 1 μm show multiple domains with dominant in-plane magnetization component. Below 1 μm, the micromagnetic configuration undergoes a transition to an in-plane vortex with core pointing outward parallel to the cylinder axis. At the perimeter the magnetization tilts toward the $x-y$ plane, but the net M_z over the whole magnet volume increases significantly. Between 750 and 300 nm the micromagnetic configuration remains essentially unchanged with a continuing increase of the out-of-plane magnetized region around the central axis and M_z. At 250 nm (AR = 0.6) the micromagnetic configuration undergoes another transition to a primarily out-of-plane magnetized single-domain structure apart from the base plane regions, where the vortexlike configuration still exists. At 125 nm, the magnet becomes fully single domain.

Since our probe spot samples the entire nanomagnet for diameters $\leq 1\ \mu$m, the average component of the magnetization parallel to the bias field must be considered for calculating the precession frequency. We have incorporated the net M_z averaged over the whole magnet volume in eq 1 to calculate the expected precession frequencies, which are shown by the solid lines (Figure 3a,b) and agree well with the experimental data. The deviation is slightly larger for

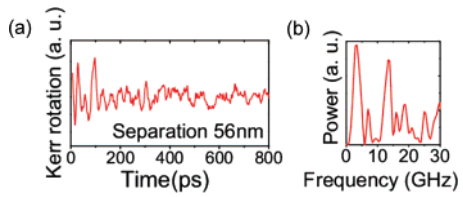

Figure 5. (a) Time-resolved Kerr rotations (raw data) for arrays of 150 nm magnets with edge to edge separation of 56 nm at H_{bias} = 1.68 kOe. (b) Double exponential background subtracted data and corresponding FFT spectra from (a).

small magnets due to greater uncertainty in determining the peak frequency and larger nonidealities such as surface roughness or finite temperature effects that could not be included in the OOMMF simulations. Both size and field dependence can be explained with a single parameter set using $K_{S2} = 0.81$ erg/cm^2 and $H_{off} = 820$ Oe. Variation of M_z and different terms in eq 1 with magnet diameter (aspect ratio) are shown (Figure 3c). The average demagnetizing fields could be independently obtained from the OOMMF simulation and would essentially give the same values as obtained when the averaged M_z is multiplied by the demagnetizing factor. We see that the general trend of increasing precession frequency with reduced magnet size is a result of the size dependence of the average demagnetizing field and surface anisotropy field. However, a combination of these two fields is not sufficient to explain the significant jump in the experimental data of Figure 3a. Instead, a change in the effective volume anisotropy constant K_1 from 1×10^4 erg/cm^3 for samples >250 nm to 1.5×10^5 erg/cm^3 for samples ≤ 250 nm needs to be taken into account. A change in crystal structure and consequently K_{uz} is unlikely. Therefore, we attribute the discontinuity to a change in the surface-related term K_{S1}, possibly resulting from surface defects and irregularities at the edges. We point out that sudden switching of the magnetic easy axis at similar aspect ratios (0.63 and 0.65) has been reported from quasi-static hysteresis loop measurements in comparable nickel nanomagnets.[35,36] The 4-fold increase in the precession frequency by reduction of magnet diameter from 2 μm to 125 nm is significant for high-speed operation of high-density magnetic storage devices. This trend is expected to continue below 125 nm (see simulated curve in Figure 3a).

The utility of single particle measurements is already evident from our ability to rule out sample (particle to particle) inhomogeneities as the reason for the observed frequency jump at AR = 0.6. As a final example, we present a direct comparison with measurements on a dense nanomagnet array from which a larger magneto-optic signal might be expected. We measured the dynamics from an array of 150 nm magnets separated by 56 nm (Figure 5a), comparable to densities found in prototype patterned storage media,[1] where magnetostatic fields from neighboring magnets cannot be neglected. The time-domain trace is noisier and the FFT spectrum (Figure 5b) shows a much broader response than for single nanomagnets (Figure 2b), likely due to particle imperfections and dynamic dephasing of the precession caused by time-varying dipole fields of neighboring magnets. These nonidealities have a greater effect on the dynamics in an array because of the highly nontrivial coupling of multiple dynamic equations.

We modeled the range of precession frequencies in the array by including (static) dipolar fields from the first two nearest neighbors (eight magnets) in H_{eff}. The gray shaded area in Figure 3a shows the expected frequency range bounded by the extreme cases of all "up" or all "down" configurations of the first two nearest neighbors. This provides an estimation of the uncertainty in quantifying the precession frequencies due to the (static) ensemble effect. We see that the step at 250 nm would be washed out significantly and may not be observable if additional fluctuations, e.g., in magnet dimension or surface quality, are present. The figure illustrates that the overall trend (higher precession frequency for smaller magnets) could be observed by array measurements, but finer structures may not be resolved. It is evident from Figures 5b and 3a that single nanomagnet measurements are necessary to identify the intrinsic response of single nanomagnets, especially at smaller length scales.

In summary, we have analyzed the dynamic properties of nanoscale magnetic materials on a picosecond time scale. Cavity-enhanced MOKE was used to substantially improve the spatiotemporal sensitivity in a noninvasive manner and enable the observation of individual single-domain magnets in our MOKE setup. We analyzed the precessional dynamics of single nanomagnets as they undergo a transition from in-plane to out-of plane magnetization. The absence of ensemble effects permitted access to the intrinsic dynamic behavior. Further optimization of CE-MOKE promises numerous additional opportunities. These include near-field detection for lateral resolution in dense arrays and modifications to the cavity enhancement process for higher sensitivity.[37] In the future, time-resolved magneto-optics will provide an essential nanocharacterization tool to explore linear and nonlinear dynamics of new materials on the shortest time scales.

Acknowledgment. We thank N. Qureshi and B. Hillebrands for fruitful discussions, the National Science Foundation (Grant ECS-0245425), and Office of Science, Office of Basic Energy Sciences, of the U.S. Department of Energy (Contract No. DE-AC02-05CH11231) for financial support.

Supporting Information Available: A schematic drawing of the experimental MOKE setup. This material is available free of charge via the Internet at http://pubs.acs.org.

References

(1) Terris, B. D.; Thomson, T. Nanofabricated *J. Phys. D*: *Appl. Phys.* **2005**, *38*, R199.
(2) Åkerman, J. *Science* **2005**, *308*, 508.
(3) Allwood, D. A.; et al. *Science* **2005**, *309*, 1688.
(4) Chung, S. H.; et al. *Appl. Phys. Lett.* **2004**, *85*, 2971.
(5) Anderson, E. A.; et al. *Nano Lett.* **2006**, *6*, 1160.
(6) McMillan, R. A.; et al. *Nature Mater.* **2002**, *1*, 247.
(7) Bean, C. P. *J. Appl. Phys.* **1955**, *26*, 1381.
(8) Hartmann, U.; Goddenhenrich, T.; Heiden *J. Magn. Magn. Mater.* **1991**, *101*, 263.
(9) Wulfhekel, W.; Kirschner, J. *Appl. Phys. Lett.* **1999**, *75*, 1944.
(10) Chapman, J. N. *J. Phys. D*: *Appl. Phys.* **1984**, *17*, 623.
(11) Poppa, H.; Bauer, E.; Pinkvos, H. *MRS Bull.* **1995**, *20*, 38.

(12) Jorzick, J.; et al. *Phys. Rev. Lett.* **2002**, *88*, 047204.
(13) Roussigne, Y.; Cherif, S. M.; Dugautier, C.; Moch, P. *Phys. Rev. B* **2001**, *63*, 134429.
(14) Jung, S.; Watkins, B.; DeLong, L.; Ketterson, J. B.; Chandrasekhar, V. *Phys. Rev. B* **2002**, *66*, 132401.
(15) Tamaru, S.; et al. *J. Appl. Phys.* **2002**, *91*, 8034.
(16) Acremann, Y.; et al. *Science* **2000**, *290*, 492.
(17) Park, J. P.; Crowell, P. A. *Phys. Rev. Lett.* **2005**, *95*, 167201.
(18) Barman, A.; Kruglyak, V. V.; Hicken, R. J.; Kundrotaite, A.; Rahman, M. *Appl. Phys. Lett.* **2003**, *82*, 3065.
(19) Zhu, X.; Malac, M.; Liu, Z.; Qian, H.; Metlushko, V.; Freeman, M. R. *Appl. Phys. Lett.* **2005**, *86*, 262502.
(20) Buchanan, K. S.; et al. *Nature Phys.* **2005**, *1*, 172.
(21) van Kampen, M.; et al. *Phys. Rev. Lett.* **2002**, *88*, 227201.
(22) Silva, T. J.; Lee, C. S.; Crawford, T. M.; Rogers, C. T. *J. Appl. Phys.* **1999**, *85*, 7849.
(23) Krivorotov, I. N.; et al. *Science* **2005**, *307*, 228.
(24) Koch, R. H.; Katine, J. A.; Sun, J. Z. *Phys. Rev. Lett.* **2004**, *92*, 088302.
(25) Acreman, Y.; et al. *Phys. Rev. Lett.* **2006**, *96*, 217202.
(26) Gubbiotti, G.; et al. *Phys. Rev. B* **2003**, *68*, 184409.
(27) Kruglyak, V. V.; Barman, A.; Hicken, R. J.; Childress, J. F.; Katine, J. A. *Phys. Rev. B* **2005**, *71*, 220409(R).
(28) Buchanan, K. S.; Zhu, X.; Meldrum, A.; Freeman, M. R. *Nano Lett.* **2005**, *5*, 383.
(29) Sokolov, A. V. *Optical Properties of Metals*; Blackie: London, 1967; p 311.
(30) Qureshi, N.; et al. *Nano Lett.* **2005**, *5*, 1413.
(31) Landau, L. D.; Lifshitz, E. *Phys. Z. Sowjetunion* **1935**, *8*, 153.
(32) Aharoni, A. *Introduction to the theory of ferromagnetism*, 2nd ed.; Oxford Science: New York, 2000; p 115.
(33) Donahue, M.; Porter, D. G. OOMMF User's guide, Version 1.0, Interagency Report NISTIR 6376, National Institute of Standard and Technology, Gaithersburg, MD (1999): URL: http://math.nist.gov/oommf.
(34) Gerrits, T.; van den Berg, H. A. M.; Hohlfeld, J.; Bär, L.; Rasing, T. *Nature* **2002**, *418*, 509.
(35) Meier, G.; Kleiber, M.; Grundler, D.; Heitmann, D.; Wiesendanger, R. *Appl. Phys. Lett.* **1998**, *72*, 2168.
(36) Ross, C. A. et al. *J. Appl. Phys.* **2001**, *89*, 1310.
(37) Wang, S.; et al. The 50th Magnetism and Magnetic Materials Conference, Abstract No. AD-11, San Jose, CA, 2005.

NL0623457